

One-dimensional topological insulator: a model for studying finite-size effects in topological insulator thin films

Mayuko Okamoto, Yositake Takane, and Ken-Ichiro Imura

Department of Quantum Matter, AdSM, Hiroshima University, Higashi-Hiroshima 739-8530, Japan

(Dated: March 7, 2014)

As a model for describing finite-size effects in topological insulator thin films, we study a one-dimensional (1D) effective model of a topological insulator (TI). Using this effective 1D model, we reveal the precise correspondence between the spatial profile of the surface wave function, and the dependence of the finite-size energy gap on the thickness (L_x) of the film. We solve the boundary problem both in the semi-infinite and slab geometries to show that the L_x -dependence of the size gap is a direct measure of the amplitude of the surface wave function $\psi(x)$ at the depth of $x = L_x + 1$ [here, the boundary condition is chosen such that $\psi(0) = \mathbf{0}$]. Depending on the parameters, the edge state function shows either a damped oscillation (in the “TI-oscillatory” region of FIG. 2), or becomes overdamped (*ibid.*, in the “TI-overdamped” phase). In the original 3D bulk TI, an asymmetry in the spectrum of valence and conduction bands is omnipresent. Here, we demonstrate by tuning this asymmetry one can drive a crossover from the TI-oscillatory to the TI-overdamped phase.

PACS numbers: 73.20.-r, 73.22.-f

I. INTRODUCTION

Existence of a protected¹⁻⁴ gapless state is a defining property of the topological insulator, which is also considered to be gapless.⁵⁻⁷ Yet, in realistic systems of a finite size, *e.g.*, in thin films of a topological insulator,⁸⁻¹² this last clause is not guaranteed by the topological protection. The magnitude of such a finite-size energy gap in the case of a thin film is naturally related to the degree of penetration of the surface state wave function into the bulk in the light of the thickness of the film.¹³⁻¹⁸ Here, in this paper we point out that this correspondence can be made more precise. Indeed, in the system considered the thickness dependence of the finite-size energy gap is shown to be a direct measure of the amplitude of the surface wave function.

II. REDUCTION OF THE 3D BULK HAMILTONIAN TO A 1D MODEL

The physical system we consider is a slab-shaped sample of three-dimensional (3D) topological insulator (TI), *i.e.*, a TI thin film, or a nanofilm. We first show in this section that finite-size effects in such TI films are described by an effective 1D model, representing a “one-dimensional topological insulator”. Here, let us go back to the bulk 3D TI, described by the following tight-binding (Wilson-Dirac type) Hamiltonian:^{19,20}

$$h_{3D}(\mathbf{k}) = \gamma_0 m(\mathbf{k}) + \gamma_\mu t_\mu \sin k_\mu + \epsilon(\mathbf{k}) \mathbf{1}_4, \quad (1)$$

where

$$m(\mathbf{k}) = m_0 + 2 \sum_{\mu=x,y,z} m_{2\mu} (1 - \cos k_\mu), \quad (2)$$

$$\epsilon(\mathbf{k}) = \epsilon_0 + 2 \sum_{\mu=x,y,z} \epsilon_{2\mu} (1 - \cos k_\mu). \quad (3)$$

γ_0 and three γ_μ 's ($\mu = x, y, z$) are a set of γ -matrices, which can be chosen as

$$\gamma_0 = \tau_z, \quad \gamma_x = \tau_x \sigma_z, \quad \gamma_y = \tau_x \sigma_x, \quad \gamma_z = \tau_x \sigma_y. \quad (4)$$

σ_μ 's ($\mu = x, y, z$) are Pauli matrices representing the real spin. $\mathbf{1}_4$ represents a 4×4 identity matrix, while the time reversal symmetry requires $m(\mathbf{k})$ and $\epsilon(\mathbf{k})$ to be an even function of \mathbf{k} . The form of the hopping (sine and cosine) terms in Eqs. (1), (2) and (3) reflects that our tight-binding Hamiltonian is implemented on a cubic lattice, and we consider only nearest neighbor hopping. Changing the mass parameters: m_0 and m_{2x}, m_{2y}, m_{2z} in Eq. (2), one can realize different types of weak and strong topological insulating phases.¹⁸

Here, in this paper we study in detail the spatial profile of the surface wave function in the semi-infinite geometry, and the finite-size energy gap in the slab geometry, to reveal a close relation between them. In the semi-infinite

geometry, the bulk 3D TI occupies the semi-infinite space $x > 0$ with a surface on the (y, z) -plane. While, in the slab the bulk 3D TI is confined to a slab-shaped region $0 < x < L_x$. In the two cases studied, the translational invariance in the y - and z -directions are respected, so that $\mathbf{k}_{\parallel} = (k_y, k_z)$ is still a good quantum number. The energy spectrum is then expressed as $E = E(\mathbf{k}_{\parallel})$, and \mathbf{k}_{\parallel} belongs to the surface Brillouin zone (BZ).

For keeping the subsequent discussions reasonably simple, we only consider the case of a slab structure commensurate with the cubic symmetry; here, we place it perpendicular to the x -axis ($\mathbf{k}_{\perp} = k_x$). Then, the cubic symmetry of the lattice and of the BZ ensures that gapless surface Dirac points appear at the four symmetric points in the surface BZ, $\bar{\Gamma} = (0, 0)$, $\bar{Y} = (\pi, 0)$, $\bar{Z} = (0, \pi)$, $\bar{M} = (\pi, \pi)$. At these symmetric points, relevant to the low-energy spectrum of the surface states, the hopping terms in the y - and z -directions become inert, *i.e.*,

$$h_{3D}(k_x, \mathbf{k}_{\parallel} = \bar{\Gamma}, \bar{Y}, \bar{Z}, \bar{M}) = \tau_z m(k_x, \mathbf{k}_{\parallel}) + \tau_x \sigma_z t_x \sin k_x, \quad (5)$$

where

$$m(k_x, \mathbf{k}_{\parallel}) = \tilde{m}_0(\mathbf{k}_{\parallel}) + 2m_{2x}(1 - \cos k_x), \quad (6)$$

with

$$\tilde{m}_0(\mathbf{k}_{\parallel}) = \begin{cases} m_0 & (\mathbf{k}_{\parallel} = \bar{\Gamma}) \\ m_0 + 2m_{2y} & (\mathbf{k}_{\parallel} = \bar{Y}) \\ m_0 + 2m_{2z} & (\mathbf{k}_{\parallel} = \bar{Z}) \\ m_0 + 2(m_{2y} + m_{2z}) & (\mathbf{k}_{\parallel} = \bar{M}) \end{cases}. \quad (7)$$

There, the 4×4 Hamiltonian matrix can be organized into a block-diagonal form as

$$h_{3D}(k_x, \mathbf{k}_{\parallel} = \bar{\Gamma}, \bar{Y}, \bar{Z}, \bar{M}) = \left[\begin{array}{cc|cc} m(k_x, \mathbf{k}_{\parallel}) & t_x \sin k_x & & \mathbf{0} \\ t_x \sin k_x & -m(k_x, \mathbf{k}_{\parallel}) & & \\ \hline & & m(k_x, \mathbf{k}_{\parallel}) & -t_x \sin k_x \\ & & -t_x \sin k_x & -m(k_x, \mathbf{k}_{\parallel}) \end{array} \right] \\ \equiv \left[\begin{array}{cc} h_{1D}(k_x) & \mathbf{0} \\ \mathbf{0} & h_{1D}(-k_x) \end{array} \right]. \quad (8)$$

As we will see explicitly in the following sections, the surface states of a slab-shaped TI with a finite thickness L_x exhibit indeed a finite-size energy gap, due to (though this is not the way how we tackle the problem) overlap of the wave functions on the top and bottom surfaces. Yet, the magnitude of this energy gap is minimal at either of these four symmetric \mathbf{k}_{\parallel} -points at which the surface spectrum becomes gapless in the ideal situation; *i.e.*, when $L_x \rightarrow \infty$ or in a semi-infinite geometry. Since the real spin down sector ($\sigma_z = -1$) is obtained from the spin up sector ($\sigma_z = 1$) by simply reversing the direction of motion, we can safely focus on the spin up sector described by the effective 1D theory represented as a 2×2 Hamiltonian matrix $h_{1D}(k_x)$.

Though this reduction to a 2×2 matrix occurs only at the four symmetric points, at each point \mathbf{k}_{\parallel} of the surface BZ, one can always attribute an effective 1D Hamiltonian, which is actually nothing but $h_{3D}(k_x, \mathbf{k}_{\parallel})$. Then, at each point \mathbf{k}_{\parallel} one solves this 1D Hamiltonian with an open (or semi-infinite) boundary condition, and in some cases one finds edge solutions as a mid gap state, generally at $E = \bar{E}_{\pm} \neq 0$, while in other cases one may find only bulk solutions. Even for a given set of model parameters (m_0 , m_{2x} , etc.) this depends on the value of \mathbf{k}_{\parallel} , since it can happen, and actually it almost always happens that an edge state merge and disappear into the bulk spectrum at some finite \mathbf{k}_{\parallel} . The spectrum of the surface state, typically taking a conic shape (a Dirac cone) around at least one of the four symmetric points is found as a locus of the energy $\bar{E}_{\pm}(\mathbf{k}_{\parallel})$ at which an edge state (if exists) appears as a solution of the corresponding 1D problem.

III. WINDING PROPERTIES OF THE 1D MODEL

Let us rewrite the effective 1D tight-binding Hamiltonian $h_{1D}(k_x)$ as

$$h_{1D}(k_x) = m(k_x)\tau_z + t_x \sin k_x \tau_x + \epsilon(k_x)1_2, \quad (9)$$

where

$$m(k_x) = m_0 + 2m_{2x}(1 - \cos k_x), \quad (10)$$

$$\epsilon(k_x) = \epsilon_0 + 2\epsilon_{2x}(1 - \cos k_x). \quad (11)$$

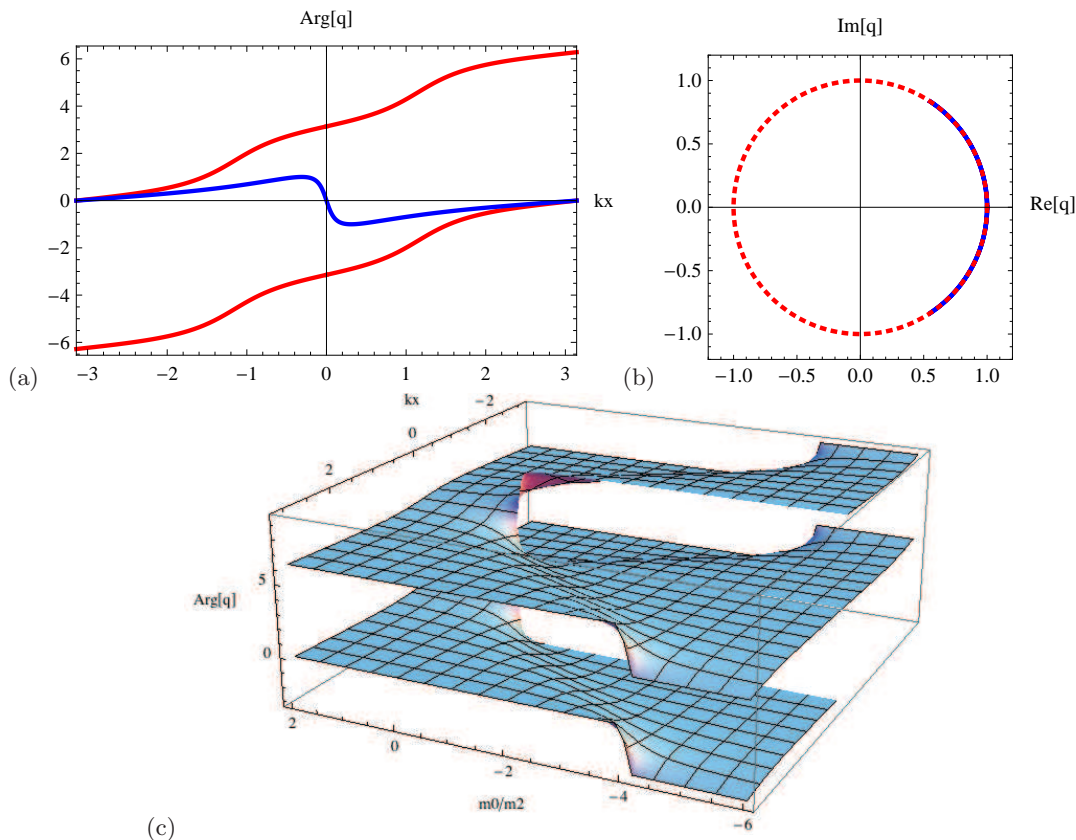


FIG. 1: Topological protection, or winding in the 1D model. (a) $\arg q$ plotted as a function of k_x in the trivial ($m_0/m_{2x} = 0.1$, blue curve) and nontrivial ($m_0/m_{2x} = -1.3$, red curve) phases. (b) locus of the points: $(\text{Re } q, \text{Im } q)$ when k_x sweeps once the entire Brillouin zone: $k_x \in [-\pi, \pi]$ [blue: $m_0/m_{2x} = 0.1$, (red, dotted): $m_0/m_{2x} = -1.3$]. (c) global behavior of $\arg q$ in the $(m_0/m_{2x}, k_x)$ -plane. When $m_0/m_{2x} \in [-4, 0]$, the winding number \mathcal{N}_1 as defined in Eq. (13) becomes nonzero.

That is to say, focusing on the case in which the surface Dirac cone appears at $\mathbf{k}_{\parallel} = \bar{\Gamma}$, we replaced $\tilde{m}_0(\mathbf{k}_{\parallel})$ in Eq. (6) with m_0 . Other cases with surface Dirac cones at different symmetric points can be discussed by reinterpreting what we show below, *i.e.*, by replacing m_0 with $\tilde{m}_0(\mathbf{k}_{\parallel})$ given in Eq. (7).

To make explicit the winding properties of 1DTI Hamiltonian (9) it is better to adopt a slightly different choice of γ -matrices in which three elements of τ Pauli matrices are permuted as $\tau_z \rightarrow \tau_x$ and $\tau_x \rightarrow \tau_y$. By setting also $\epsilon(k_x) = 0$, one can rewrite h_{1D} in the following convenient form with vanishing diagonal components:

$$\begin{aligned} \tilde{h}_{1D}(k_x) &= m(k_x)\tau_x + t_x \sin k_x \tau_y \\ &= \begin{bmatrix} 0 & q(k_x) \\ q(k_x)^* & 0 \end{bmatrix}, \end{aligned} \quad (12)$$

where $q(k_x) = m(k_x) - it_x \sin k_x$. Then, by choosing an appropriate branch for $\phi = \arg q$ such that ϕ becomes continuous over the entire BZ: $k_x \in [-\pi, \pi]$ one can introduce a winding number \mathcal{N}_1 such that

$$\mathcal{N}_1 = \frac{\phi(k_x = \pi) - \phi(k_x = -\pi)}{2\pi}, \quad (13)$$

associated with a mapping from S^1 to S^1 [mapping from the 1D BZ to a (unit) circle in the complex q -plane]. The nontrivial winding of $q(k_x)$ is depicted in FIG. 1. One can indeed explicitly verify

$$\mathcal{N}_1 = \begin{cases} 1 & (-4 < m_0/m_{2x} < 0) \\ 0 & (\text{otherwise}) \end{cases}. \quad (14)$$

As we see explicitly in the next section (see also FIG. 2, the phase diagram determined by the presence/absence/nature of the edge solution), whenever the winding number \mathcal{N}_1 takes a nontrivial value ($\mathcal{N}_1 = 1$), there appears a zero-energy

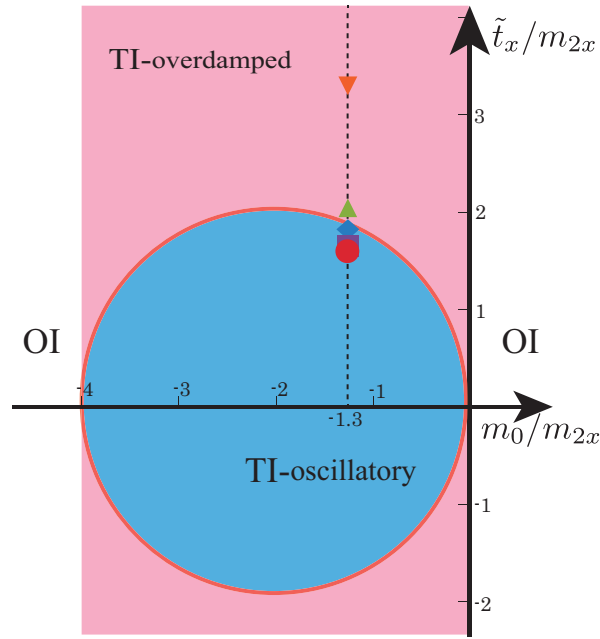


FIG. 2: Phase diagram of the 1D topological insulator in the space of mass and hopping parameters $[(m_0/m_{2x}, \tilde{t}_x/m_{2x})$ -plane]. As given in Eq. (45) \tilde{t}_x is a function of ϵ_{2x} . The latter encodes asymmetry of the valence and conduction bands [see Eq. (3)].

and Γ^\dagger are (nearest-neighbor) hopping matrix elements. The corresponding eigenvalue equation,

$$H\psi = E\psi, \quad \psi = \begin{bmatrix} \vdots \\ \psi_0 \\ \psi_1 \\ \psi_2 \\ \psi_3 \\ \vdots \end{bmatrix} \quad (20)$$

has a solution of the form:

$$\psi_j = \psi_j[\rho] = \rho^j \mathbf{u}. \quad (21)$$

Here, \mathbf{u} is a two-component (eigen) spinor, satisfying

$$h[\rho]\mathbf{u} = E\mathbf{u}, \quad (22)$$

where

$$h[\rho] = \epsilon[\rho]1_2 + m[\rho]\tau_z + t_x \frac{\rho - \rho^{-1}}{2i} \tau_x, \quad (23)$$

and $m[\rho] = m_0 + 2m_{2x}(1 - \frac{\rho + \rho^{-1}}{2})$, $\epsilon[\rho] = \epsilon_0 + 2\epsilon_{2x}(1 - \frac{\rho + \rho^{-1}}{2})$. Eq. (22) with Eq. (23) is nothing but the eigenvalue equation for $h(k_x)$ in momentum space, if ρ is expressed as $\rho = e^{ik_x}$. For a given energy E , the secular equation, $\det(h[\rho] - E) = 0$ gives, generally, four solutions for $\rho = \rho_A, \rho_B, \rho_C, \rho_D$, and the corresponding eigenvectors, $\mathbf{u} = u_A, u_B, u_C, u_D$.

Under a periodic boundary condition: $\psi_N = \psi_0$, $\rho^N = 1$, implying $|\rho| = 1$, or $\rho = e^{ik_x}$ with k_x : real and given as $k_x = \frac{2\pi}{N}n$ with $n = 0, \pm 1, \pm 2, \dots$. For a given k_x , the corresponding energy eigenvalue is given as

$$E = E(k_x) = \epsilon(k_x) \pm \sqrt{m(k_x)^2 + t^2 \sin^2 k_x}. \quad (24)$$

B. Construction of the edge solutions

Let us consider the case of a semi-infinite geometry: $x > 0$, in which the edge solution ψ as introduced in Eq. (20) has a finite amplitude ψ_j on site $x = j \geq 1$ that decays also exponentially as $j \rightarrow +\infty$, *i.e.*,

$$\psi_0 = \begin{bmatrix} 0 \\ 0 \end{bmatrix}, \quad \psi(x \rightarrow +\infty) = \begin{bmatrix} 0 \\ 0 \end{bmatrix}, \quad (25)$$

Such a solution is given by a difference of two solutions of the type given in Eq. (21):

$$\psi_j = \left(\rho_A^j - \rho_B^j \right) \mathbf{u}, \quad (26)$$

with $\rho_A \neq \rho_B$, $|\rho_A| < 1$, $|\rho_B| < 1$. Also, $\mathbf{u}_A = \mathbf{u}_B \equiv \mathbf{u}$ is implicit in Eq. (26); therefore, in the following we search for solutions of the type of Eq. (21) with different ρ but with the same eigenspinor \mathbf{u} . In other words, we need a simultaneous solution of

$$\begin{aligned} (h[\rho_A] - E) \mathbf{u} &= \begin{bmatrix} 0 \\ 0 \end{bmatrix}, \\ (h[\rho_B] - E) \mathbf{u} &= \begin{bmatrix} 0 \\ 0 \end{bmatrix}. \end{aligned} \quad (27)$$

These can be rewritten in the following form:

$$\begin{aligned} \frac{h[\rho_A] - E}{\gamma[\rho_A]} \mathbf{u} &= \begin{bmatrix} A_+ & -i \\ -i & -A_- \end{bmatrix} \mathbf{u} = \begin{bmatrix} 0 \\ 0 \end{bmatrix}, \\ \frac{h[\rho_B] - E}{\gamma[\rho_B]} \mathbf{u} &= \begin{bmatrix} B_+ & -i \\ -i & -B_- \end{bmatrix} \mathbf{u} = \begin{bmatrix} 0 \\ 0 \end{bmatrix}, \end{aligned} \quad (28)$$

where

$$\begin{aligned} A_+ &= \frac{m_A - (E - \epsilon_A)}{\gamma_A}, \quad B_+ = \frac{m_B - (E - \epsilon_B)}{\gamma_B} \\ A_- &= \frac{m_A + E - \epsilon_A}{\gamma_A}, \quad B_- = \frac{m_B + E - \epsilon_B}{\gamma_B}. \end{aligned} \quad (29)$$

Here, m_A , m_B , ϵ_A and ϵ_B , are short-hand notations for $m[\rho_A]$, $m[\rho_B]$, $\epsilon[\rho_A]$ and $\epsilon[\rho_B]$. We have also introduced,

$$\gamma[\rho] = t_x \frac{\rho - \rho^{-1}}{2}, \quad (30)$$

and $\gamma_A = \gamma[\rho_A]$, $\gamma_B = \gamma[\rho_B]$. Clearly, the two eigenvalue equations share the same eigenvector \mathbf{u} only when $A_+ = B_+$ and $A_- = B_-$, implying

$$\frac{m_A - (E - \epsilon_A)}{m_A + E - \epsilon_A} = \frac{m_B - (E - \epsilon_B)}{m_B + E - \epsilon_B}. \quad (31)$$

This condition imposed by the semi-infinite geometry, or by the boundary condition (25) plays the role of determining the energy E at which an edge state appears; Eq. (31) first simplifies to

$$m_A(E - \epsilon_B) = m_B(E - \epsilon_A). \quad (32)$$

Then, recalling $m_A = m_0 + m_{2x}k_A^2$, $m_B = m_0 + m_{2x}k_B^2$, $\epsilon_A = \epsilon_0 + \epsilon_{2x}k_A^2$ and $\epsilon_B = \epsilon_0 + \epsilon_{2x}k_B^2$, where k_A^2 and k_B^2 are short-hand notations for $k_A^2 = 2(1 - \frac{\rho_A + \rho_A^{-1}}{2})$ and $k_B^2 = 2(1 - \frac{\rho_B + \rho_B^{-1}}{2})$, one finds,

$$(k_A^2 - k_B^2)\{m_0\epsilon_{2x} + m_{2x}(E - \epsilon_0)\} = 0. \quad (33)$$

Since $\rho_A \neq \rho_B$, this means,¹⁶

$$E = \epsilon_0 - \frac{m_0}{m_{2x}}\epsilon_{2x} \equiv \bar{E}, \quad (34)$$

and this is the energy at which an edge state appears. In the special case of $\epsilon(k_x) = 0$ (particle-hole symmetric case), this reduces to a simple zero-energy condition: $E = 0$, while here, in the presence of $\epsilon(k_x) \neq 0$, this condition is relaxed. Eq. (34) also implies that at this energy $E = \bar{E}$ the two independent parameters $\epsilon[\rho] - E$ and $m[\rho]$ have the same functional form:

$$\epsilon[\rho] - \bar{E} = \frac{\epsilon_{2x}}{m_{2x}} m[\rho]. \quad (35)$$

Let us go back to the eigenvalue equation: Eq. (22), or Eqs. (27), and find the corresponding eigenvector. Let us recall

$$h[\rho] - E = \begin{bmatrix} m[\rho] + \epsilon[\rho] - E & -i\gamma[\rho] \\ -i\gamma[\rho] & -(m[\rho] - \epsilon[\rho] + E) \end{bmatrix} \quad (36)$$

Then, from the secular equation: $\det(h[\rho] - E) = 0$, one must have,

$$\gamma[\rho] = \pm \sqrt{m[\rho]^2 - (E - \epsilon[\rho])^2} \equiv \gamma_{1,2}, \quad (37)$$

The subscripts of γ corresponds to the two choices of sign in front of the square root in the middle expression. At $E = \bar{E}$, Eq. (35) implies

$$\gamma[\rho] = \gamma_{1,2}[\rho] = \pm \sqrt{1 - \frac{\epsilon_{2x}^2}{m_{2x}^2} m[\rho]}, \quad (38)$$

i.e., $\gamma[\rho]$ also shares the same functional form as $m[\rho]$. But here, let us continue expressing γ 's as in Eq. (37), and rewrite Eqs. (28) as

$$\frac{h_{1,2} - E}{\gamma_{1,2}} \mathbf{u}_{1,2} = \begin{bmatrix} \pm \sqrt{\frac{m+\epsilon-E}{m-\epsilon+E}} & -i \\ -i & \mp \sqrt{\frac{m-\epsilon+E}{m+\epsilon-E}} \end{bmatrix} \mathbf{u}_{1,2} = \begin{bmatrix} 0 \\ 0 \end{bmatrix}. \quad (39)$$

Here, we introduced the notation $h_{1,2}$ such that $h = h_{1,2}$ when $\gamma = \gamma_{1,2}$. The corresponding eigenvectors $\mathbf{u}_{1,2}$ are found (up to normalization, *i.e.*, $|\mathbf{u}_1|^2 = |\mathbf{u}_2|^2 = 1$) as

$$\mathbf{u}_1 = \frac{1}{\sqrt{2m}} \begin{bmatrix} \sqrt{m - \epsilon + E} \\ -i\sqrt{m + \epsilon - E} \end{bmatrix}, \quad (40)$$

$$\mathbf{u}_2 = \frac{1}{\sqrt{2m}} \begin{bmatrix} \sqrt{m - \epsilon + E} \\ i\sqrt{m + \epsilon - E} \end{bmatrix}. \quad (41)$$

where $m = m[\rho]$ and $\epsilon = \epsilon[\rho]$ are functions of ρ , and through $\rho = \rho(E)$ they are also functions of E . At $E = \bar{E}$ these reduce to

$$\mathbf{u}_1^{(0)} = \frac{1}{\sqrt{2}} \begin{bmatrix} \sqrt{1 - \frac{\epsilon_{2x}}{m_{2x}}} \\ -i\sqrt{1 + \frac{\epsilon_{2x}}{m_{2x}}} \end{bmatrix}, \quad (42)$$

$$\mathbf{u}_2^{(0)} = \frac{1}{\sqrt{2}} \begin{bmatrix} \sqrt{1 - \frac{\epsilon_{2x}}{m_{2x}}} \\ i\sqrt{1 + \frac{\epsilon_{2x}}{m_{2x}}} \end{bmatrix}. \quad (43)$$

The identity: $\gamma[\rho] = \gamma_1[\rho] = \sqrt{1 - \frac{\epsilon_{2x}^2}{m_{2x}^2} m[\rho]}$ in Eq. (38), can be viewed as a quadratic equation for ρ , *i.e.*, $a\rho^2 + b\rho + c = 0$ with

$$a = m_{2x} + \tilde{t}_x/2, \quad b = -(m_0 + 2m_{2x}), \quad c = m_{2x} - \tilde{t}_x/2, \quad (44)$$

where

$$\tilde{t}_x = \frac{t_x}{\sqrt{1 - \frac{\epsilon_{2x}^2}{m_{2x}^2}}} \quad (45)$$

represents rescaled hopping. Let us name the two solutions of this quadratic equation as

$$\rho = \rho_{1\pm} = \frac{m_0 + 2m_{2x} \pm \sqrt{(m_0 + 2m_{2x})^2 - 4(m_{2x}^2 - \tilde{t}_x^2/4)}}{2(m_{2x} + \tilde{t}_x/2)}. \quad (46)$$

The second choice for γ in Eq. (38), *i.e.*, $\gamma[\rho] = \gamma_2[\rho] = -\sqrt{1 - \frac{\epsilon_{2x}^2}{m_{2x}^2}}m[\rho]$ replaces Eqs. (44) with

$$a = m_{2x} - \tilde{t}_x/2, \quad b = -(m_0 + 2m_{2x}), \quad c = m_{2x} + \tilde{t}_x/2, \quad (47)$$

i.e., \tilde{t}_x is replaced with $-\tilde{t}_x$. This leads to the second set of solutions for ρ :

$$\rho = \rho_{2\pm} = \frac{m_0 + 2m_{2x} \pm \sqrt{(m_0 + 2m_{2x})^2 - 4(m_{2x}^2 - \tilde{t}_x^2/4)}}{2(m_{2x} - \tilde{t}_x/2)}. \quad (48)$$

The case of $m_{2x} \pm \tilde{t}_x/2 = 0$ may need a separate consideration.

Case of $D = b^2 - 4ac < 0$: a pair of complex conjugate solutions; the two solutions for ρ become a pair of mutually conjugate complex numbers,

$$\rho = \frac{-b \pm i\sqrt{4ac - b^2}}{2a}. \quad (49)$$

Therefore,

$$|\rho|^2 = \frac{b^2 + 4ac - b^2}{4a^2} = \frac{c}{a} = \frac{m_{2x} \mp \tilde{t}_x/2}{m_{2x} \pm \tilde{t}_x/2} \quad (50)$$

If one sets the parameters such that $m_{2x} > 0$ and $t_x > 0$, one must have

$$|\rho_{1\pm}| < 1, \quad |\rho_{2\pm}| > 1. \quad (51)$$

Then, since $\rho = \rho_{1\pm}$ share the same eigenspinor $\mathbf{u}_1^{(0)}$, choosing in Eq. (26) as $\rho_A = \rho_{1+}$ and $\rho_B = \rho_{1-}$, we find that

$$\psi_{\text{semi}} = \begin{bmatrix} \psi_0 \\ \psi_1 \\ \psi_2 \\ \psi_3 \\ \vdots \end{bmatrix} \quad (52)$$

with

$$\begin{aligned} \psi_j &= \mathcal{N} (\rho_{1+}^j - \rho_{1-}^j) \mathbf{u}_1 \\ &= \frac{\mathcal{N}}{\sqrt{2}} (\rho_{1+}^j - \rho_{1-}^j) \begin{bmatrix} \sqrt{1 - \frac{\epsilon_{2x}}{m_{2x}}} \\ -i\sqrt{1 + \frac{\epsilon_{2x}}{m_{2x}}} \end{bmatrix}. \end{aligned} \quad (53)$$

(for $j = 0, 1, 2, 3, \dots$) is the edge/surface solution in the semi-infinite geometry that appears at $E = \bar{E} = \epsilon_0 + \frac{m_0}{m_{2x}}\epsilon_{2x}$ as given in Eq. (34). \mathcal{N} is a normalization constant. A pair of complex conjugate solutions for ρ implies that the profile of the edge/surface wave function as specified by Eqs. (52) and (53) shows a *damped oscillation*. FIG. 2 depicts the phase diagram of our 1D topological insulator, which indicates the region of parameters in which such an edge/surface wave function with a damped oscillatory profile appears. As implied in Eqs. (46) and (48) such a region is represented by the interior of a circle:

$$\left(\frac{m_0}{m_{2x}} + 2\right)^2 + \left(\frac{\tilde{t}_x}{m_{2x}}\right)^2 = 4, \quad (54)$$

in the $(m_0/m_{2x}, \tilde{t}_x/m_{2x})$ -space. In FIG. 2 this region is denoted as ‘‘TI-oscillatory’’, and painted in pale blue.

Case of $D = b^2 - 4ac > 0$: two real solutions. In this case the two solutions for ρ in Eqs. (46) and (48) become two real solutions. One can verify that the inequality (51) still holds. The edge solution: (52) with (53) is also formally unchanged, but now the wave function is *overdamped*. The corresponding parameter region in the $(m_0/m_{2x}, \tilde{t}_x/m_{2x})$ -space is the intersection of the exterior of the circle represented by Eq. 54 and the strip region: $-4 \leq m_0/m_{2x} \leq 0$. In the phase diagram of FIG. 2 this region is denoted as ‘‘TI-overdamped’’, and painted in pink.

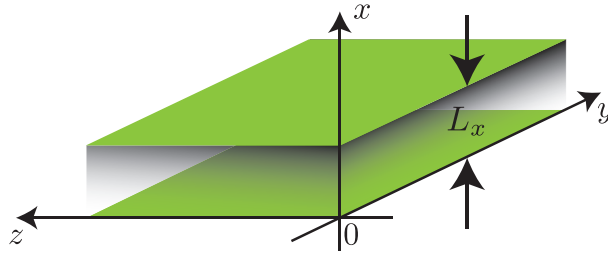


FIG. 3: The slab geometry. TI nanofilm of a thickness L_x [= the number of (quintuple) layers stacked].

V. FINITE-SIZE ENERGY GAP IN THE SLAB

Let us now generalize the previous construction of the surface wave function developed in the case of semi-infinite geometry to a more realistic case of the slab with a finite thickness L_x ; the topological insulator occupies the region of $1 \leq x \leq L_x$ (see FIG. 3). The same applies to our 1D effective model. As a result of an explicit construction, we find an (unusually) intimate relation between the magnitude of the gap and the profile of the surface wave function.¹⁸ Here, instead of Eqs. (25) we apply the following boundary condition:

$$\psi_0 = \begin{bmatrix} 0 \\ 0 \end{bmatrix}, \quad \psi_{L_x+1} = \begin{bmatrix} 0 \\ 0 \end{bmatrix}. \quad (55)$$

In this slab geometry, the asymptotic condition at $x \rightarrow +\infty$ [the second condition in Eqs. (25)] is no longer effective; so the solution of the boundary problem is expressed as a linear combination of the exponentially increasing and decreasing solutions.

We have seen earlier that \bar{E} given as in Eq. (34) is the energy of the edge solution in the semi-infinite geometry. At this energy $E = \bar{E}$, the edge solution: Eq. (52) with Eq. (53) was constructed by superposing two exponentially decreasing functions specified by $\rho_{1\pm}$ [given in Eq. (46)] and by $\mathbf{u}_1^{(0)}$ [given in Eqs. (42)]. The remaining set of solutions [that are not compatible with the boundary condition (25) and specified by $\rho_{2\pm}$ as given in Eq. (48) and by $\mathbf{u}_2^{(0)}$ as given in Eqs. (43)] are exponentially increasing functions. At $E = \bar{E}$, these two purely exponentially decreasing and increasing solutions were orthogonal to each other [see Eqs. (42) and (43)]. This, in turn, implies that in the slab geometry the energy E of the edge solution must deviate from \bar{E} ; in the present case of a slab, one needs, to cope with the boundary condition (55), to superpose both the exponentially decreasing and increasing solutions, but at $E = \bar{E}$ this was precisely not possible because of the orthogonality of $\mathbf{u}_1^{(0)}$ and $\mathbf{u}_2^{(0)}$. In the following, we attempt to construct an edge solution compatible with the boundary condition (55) by superposing exponentially decreasing and increasing solutions at E away from but still close to \bar{E} .

To be more specific, we first expand the eigenvector $\mathbf{u}_{1,2}$ as given in Eqs. (40) and (41) around $E = \bar{E}$, then by taking into account the first order corrections to $\mathbf{u}_{1,2}^{(0)}$ (in powers of $E - \bar{E}$) we attempt to construct an edge solution compatible with the boundary condition (55). Denoting as $E = \bar{E} + \delta E$, let us also expand $m = m[\rho]$ and $\epsilon = \epsilon[\rho]$ as $m = \bar{m} + \delta m$ and $\epsilon = \bar{\epsilon} + \delta \epsilon$. Here, δm and $\delta \epsilon$ denote corrections of order δE . Taking these into account one can expand each component of Eqs. (40) and (41) as

$$\begin{aligned} \sqrt{\frac{m - \epsilon + E}{m}} &\simeq \sqrt{\left(1 - \frac{\epsilon_{2x}}{m_{2x}}\right)} \left[1 + \frac{\delta E - \delta \epsilon + \frac{\epsilon_{2x} - \delta m}{m_{2x}}}{2\bar{m} \left(1 - \frac{\epsilon_{2x}}{m_{2x}}\right)} \right] \\ &= \sqrt{\left(1 - \frac{\epsilon_{2x}}{m_{2x}}\right)} \left[1 + \frac{\delta E}{2\bar{m} \left(1 - \frac{\epsilon_{2x}}{m_{2x}}\right)} \right], \end{aligned} \quad (56)$$

$$\begin{aligned} \sqrt{\frac{m + \epsilon - E}{m}} &\simeq \sqrt{\left(1 + \frac{\epsilon_{2x}}{m_{2x}}\right)} \left[1 - \frac{\delta E - \delta \epsilon + \frac{\epsilon_{2x} - \delta m}{m_{2x}}}{2\bar{m} \left(1 + \frac{\epsilon_{2x}}{m_{2x}}\right)} \right] \\ &= \sqrt{\left(1 + \frac{\epsilon_{2x}}{m_{2x}}\right)} \left[1 - \frac{\delta E}{2\bar{m} \left(1 + \frac{\epsilon_{2x}}{m_{2x}}\right)} \right]. \end{aligned} \quad (57)$$

In deriving Eqs. (56), (57) we have used the relation (35), and in simplifying the expressions, we have also noticed,

$$\delta\epsilon = \frac{\epsilon_{2x}}{m_{2x}} \delta m. \quad (58)$$

This follows immediately from the definition of m and ϵ : $m[\rho] = m_0 + 2m_{2x}(\rho + \rho^{-1})$, $\epsilon[\rho] = \epsilon_0 + 2\epsilon_{2x}(\rho + \rho^{-1})$, since these imply, $\delta m[\rho] = 2m_{2x}\delta(\rho + \rho^{-1})$, and $\delta\epsilon[\rho] = 2\epsilon_{2x}\delta(\rho + \rho^{-1})$, suggesting Eq. (58). Here, ρ should be also expanded up to linear order in δE as $\rho = \bar{\rho} + \delta\rho$. Using Eqs. (56), (57), one can rewrite $\mathbf{u}_{1,2}$ as

$$\begin{aligned} \mathbf{u}_1 &= \frac{1}{\sqrt{2m}} \begin{bmatrix} \sqrt{m - \epsilon + E} \\ -i\sqrt{m + \epsilon - E} \end{bmatrix} \\ &\simeq \frac{1}{\sqrt{2}} \begin{bmatrix} \sqrt{1 - \frac{\epsilon_{2x}}{m_{2x}}} \\ -i\sqrt{1 + \frac{\epsilon_{2x}}{m_{2x}}} \end{bmatrix} + \frac{\delta E}{2\bar{m}[\rho]\sqrt{1 - \left(\frac{\epsilon_{2x}}{m_{2x}}\right)^2}} \frac{1}{\sqrt{2}} \begin{bmatrix} \sqrt{1 + \frac{\epsilon_{2x}}{m_{2x}}} \\ i\sqrt{1 - \frac{\epsilon_{2x}}{m_{2x}}} \end{bmatrix} \\ &\equiv \mathbf{u}_1^{(0)} + \frac{\delta E}{2\bar{m}[\rho]\sqrt{1 - \left(\frac{\epsilon_{2x}}{m_{2x}}\right)^2}} \tilde{\mathbf{u}}_2, \end{aligned} \quad (59)$$

$$\begin{aligned} \mathbf{u}_2 &= \frac{1}{\sqrt{2m}} \begin{bmatrix} \sqrt{m - \epsilon + E} \\ i\sqrt{m + \epsilon - E} \end{bmatrix} \\ &\simeq \frac{1}{\sqrt{2}} \begin{bmatrix} \sqrt{1 - \frac{\epsilon_{2x}}{m_{2x}}} \\ i\sqrt{1 + \frac{\epsilon_{2x}}{m_{2x}}} \end{bmatrix} + \frac{\delta E}{2\bar{m}[\rho]\sqrt{1 - \left(\frac{\epsilon_{2x}}{m_{2x}}\right)^2}} \frac{1}{\sqrt{2}} \begin{bmatrix} \sqrt{1 + \frac{\epsilon_{2x}}{m_{2x}}} \\ -i\sqrt{1 - \frac{\epsilon_{2x}}{m_{2x}}} \end{bmatrix} \\ &\equiv \mathbf{u}_2^{(0)} + \frac{\delta E}{2\bar{m}[\rho]\sqrt{1 - \left(\frac{\epsilon_{2x}}{m_{2x}}\right)^2}} \tilde{\mathbf{u}}_1. \end{aligned} \quad (60)$$

The last lines define $\tilde{\mathbf{u}}_1$ and $\tilde{\mathbf{u}}_2$. They reduce, respectively, to $\mathbf{u}_1^{(0)}$ and $\mathbf{u}_2^{(0)}$ in the limit: $\epsilon_{2x} \rightarrow 0$, while generally this is not the case. In Eqs. (59) and (60), m and \bar{m} are functions of ρ ; they take different values in the two expressions, while even in the same expression for \mathbf{u}_1 they differ for $\rho = \rho_{1+}$ and for $\rho = \rho_{1-}$. To specify this point, we add subscripts $1\pm, 2\pm$ to \bar{m} as $\bar{m}_{1\pm}$ and $\bar{m}_{2\pm}$, and also to $\mathbf{u}_{1,2}$ as $\mathbf{u}_{1\pm}$ and $\mathbf{u}_{2\pm}$ in the following expressions. Also, ρ in $\bar{m}[\rho]$ in the denominator of the second term of Eqs. (59) and (60) is generally a function of E . But here, since the term itself is already first order in δE , we can safely replace this with the value of Eqs. (46) and (48) found at $E = \bar{E}$.

Armed with these basic solutions, we can now construct a wave function compatible with the boundary condition (55) in the spirit of Eq. (53). But here, both the exponentially increasing and decreasing solutions must be taken into account. Let us consider the superposition:

$$\psi_j = c_{1+}\rho_{1+}^j \mathbf{u}_{1+} - c_{1-}\rho_{1-}^j \mathbf{u}_{1-} + c_{2+}\rho_{2+}^{j-L_x-1} \mathbf{u}_{2+} - c_{2-}\rho_{2-}^{j-L_x-1} \mathbf{u}_{2-}. \quad (61)$$

Here, we have taken into account that the eigenspinor $\mathbf{u}_{1\pm}$ are no longer generally identical. The coefficients $c_{1\pm}, c_{2\pm}$ are to be determined so that the above ψ is compatible with the boundary condition (55). Using the expansions (59) and (60), we can rewrite Eq. (61) as

$$\begin{aligned} \psi_j &= \left(c_{1+}\rho_{1+}^j - c_{1-}\rho_{1-}^j \right) \mathbf{u}_1^{(0)} + \left(c_{1+}\frac{\rho_{1+}^j}{2\bar{m}_{1+}} - c_{1-}\frac{\rho_{1-}^j}{2\bar{m}_{1-}} \right) \frac{\delta E}{\sqrt{1 - \left(\frac{\epsilon_{2x}}{m_{2x}}\right)^2}} \tilde{\mathbf{u}}_2 \\ &+ \left(c_{2+}\rho_{2+}^{j-L_x-1} - c_{2-}\rho_{2-}^{j-L_x-1} \right) \mathbf{u}_2^{(0)} + \left(c_{2+}\frac{\rho_{2+}^{j-L_x-1}}{2\bar{m}_{2+}} - c_{2-}\frac{\rho_{2-}^{j-L_x-1}}{2\bar{m}_{2-}} \right) \frac{\delta E}{\sqrt{1 - \left(\frac{\epsilon_{2x}}{m_{2x}}\right)^2}} \tilde{\mathbf{u}}_1. \end{aligned} \quad (62)$$

Let us impose the boundary condition (55) to the above general formal form for ψ_j given as in (61). Noticing the

relations

$$\begin{aligned}
\mathbf{u}_1^{(0)\dagger} \mathbf{u}_1^{(0)} &= 1, \\
\mathbf{u}_1^{(0)\dagger} \tilde{\mathbf{u}}_2^{(0)} &= 0, \\
\mathbf{u}_1^{(0)\dagger} \mathbf{u}_2^{(0)} &= -\frac{\epsilon_{2x}}{m_{2x}}, \\
\tilde{\mathbf{u}}_2^{(0)\dagger} \mathbf{u}_1^{(0)} &= 0, \\
\tilde{\mathbf{u}}_2^{(0)\dagger} \tilde{\mathbf{u}}_2^{(0)} &= 1, \\
\tilde{\mathbf{u}}_2^{(0)\dagger} \mathbf{u}_2^{(0)} &= \sqrt{1 - \left(\frac{\epsilon_{2x}}{m_{2x}}\right)^2},
\end{aligned} \tag{63}$$

and at the leading order of $\rho_{1\pm}^{L_x}, \rho_{2\pm}^{-L_x}$ and δE (here, we consider the case of $|\rho_{1\pm}| < 1$), the original boundary problem (55) reduces to the following linear system for the four unknown coefficients $c_{1\pm}$ and $c_{2\pm}$:

$$\begin{bmatrix}
1 & -1 & -\frac{\epsilon_{2x}}{m_{2x}} \rho_{2+}^{-L_x-1} & \frac{\epsilon_{2x}}{m_{2x}} \rho_{2-}^{-L_x-1} \\
\frac{1}{2\bar{m}_{1+}} \frac{\delta E}{1 - \left(\frac{\epsilon_{2x}}{m_{2x}}\right)^2} & -\frac{1}{2\bar{m}_{1-}} \frac{\delta E}{1 - \left(\frac{\epsilon_{2x}}{m_{2x}}\right)^2} & \frac{\epsilon_{2x}}{m_{2x}} \rho_{2+}^{-L_x-1} & \frac{\epsilon_{2x}}{m_{2x}} \rho_{2-}^{-L_x-1} \\
-\frac{\epsilon_{2x}}{m_{2x}} \rho_{1+}^{L_x+1} & \frac{\epsilon_{2x}}{m_{2x}} \rho_{1-}^{L_x+1} & 1 & -1 \\
\rho_{1+}^{L_x+1} & -\rho_{1-}^{L_x+1} & \frac{1}{2\bar{m}_{2+}} \frac{\delta E}{1 - \left(\frac{\epsilon_{2x}}{m_{2x}}\right)^2} & -\frac{1}{2\bar{m}_{2-}} \frac{\delta E}{1 - \left(\frac{\epsilon_{2x}}{m_{2x}}\right)^2}
\end{bmatrix}
\begin{bmatrix}
c_{1+} \\
c_{1-} \\
c_{2+} \\
c_{2-}
\end{bmatrix}
=
\begin{bmatrix}
0 \\
0 \\
0 \\
0
\end{bmatrix}. \tag{64}$$

Finally, we solve the secular equation [(the determinant of the coefficient matrix of Eq. (64)) = 0] for δE to find the magnitude the finite-size gap. Solving the secular equation, we recall the relations such as

$$\begin{aligned}
\rho_{2\pm}^{-1} &= \rho_{1\mp}, \\
\bar{m}_{1\pm} = \gamma_{1\pm} &= \frac{\tilde{t}_x}{2} (\rho_{1\pm} - \rho_{1\pm}^{-1}) \\
&= \frac{\tilde{t}_x}{2} (\rho_{2\mp}^{-1} - \rho_{2\mp}) = -\gamma_{2\mp} = \bar{m}_{2\mp}.
\end{aligned} \tag{65}$$

One finds

$$\begin{aligned}
\delta E &= \pm 2 \left\{ 1 - \left(\frac{\epsilon_{2x}}{m_{2x}}\right)^2 \right\} \frac{\rho_{1-}^{L_x+1} - \rho_{1+}^{L_x+1}}{\frac{1}{\bar{m}_{1-}} - \frac{1}{\bar{m}_{1+}} \mp \frac{\epsilon_{2x}}{m_{2x}} \left(\frac{\rho_{1+}^{L_x+1}}{\bar{m}_{1-}} - \frac{\rho_{1-}^{L_x+1}}{\bar{m}_{1+}} \right)} \\
&= \pm 2 \left\{ 1 - \left(\frac{\epsilon_{2x}}{m_{2x}}\right)^2 \right\} \frac{\rho_{2+}^{-L_x-1} - \rho_{2-}^{-L_x-1}}{\frac{1}{\bar{m}_{2+}} - \frac{1}{\bar{m}_{2-}} \mp \frac{\epsilon_{2x}}{m_{2x}} \left(\frac{\rho_{2-}^{-L_x-1}}{\bar{m}_{2+}} - \frac{\rho_{2+}^{-L_x-1}}{\bar{m}_{2-}} \right)} \equiv \delta E_{\pm}.
\end{aligned} \tag{66}$$

Note that the second term in the denominator of Eq. (66) is much smaller than the first term, and in most cases irrelevant. When this is the case, one may convince oneself by comparing Eq. (66) and Eq. (53), that the magnitude of the finite-size energy gap $|\delta E_+ - \delta E_-| \equiv 2E_0$ in the slab of a thickness L_x is directly proportional to the amplitude of the wave function at the depth of $x = L_x + 1$,¹⁸ *i.e.*,

$$2E_0(L_x) \simeq \frac{4}{\mathcal{N}} \frac{1 - \left(\frac{\epsilon_{2x}}{m_{2x}}\right)^2}{\left| \frac{1}{\bar{m}_{1+}} - \frac{1}{\bar{m}_{1-}} \right|} |\psi_{\text{semi}}(x = L_x + 1)|. \tag{67}$$

Here, ψ_{semi} represents the surface wave function in the semi-infinite geometry as given in Eq. (52). Eqs. (66) and (67), together with the formulas for the phase boundary [Eqs. (45) and (54)] constitute the central result of this paper.

VI. COMPARISON OF ANALYTIC VS. NUMERICAL RESULTS

To check the validity of the analyses in the preceding sections let us compare the finite-size energy gap obtained numerically in slab-shaped samples with the formulas we found so far [Eqs. (45), (54), (66) and (67)]. Let us consider

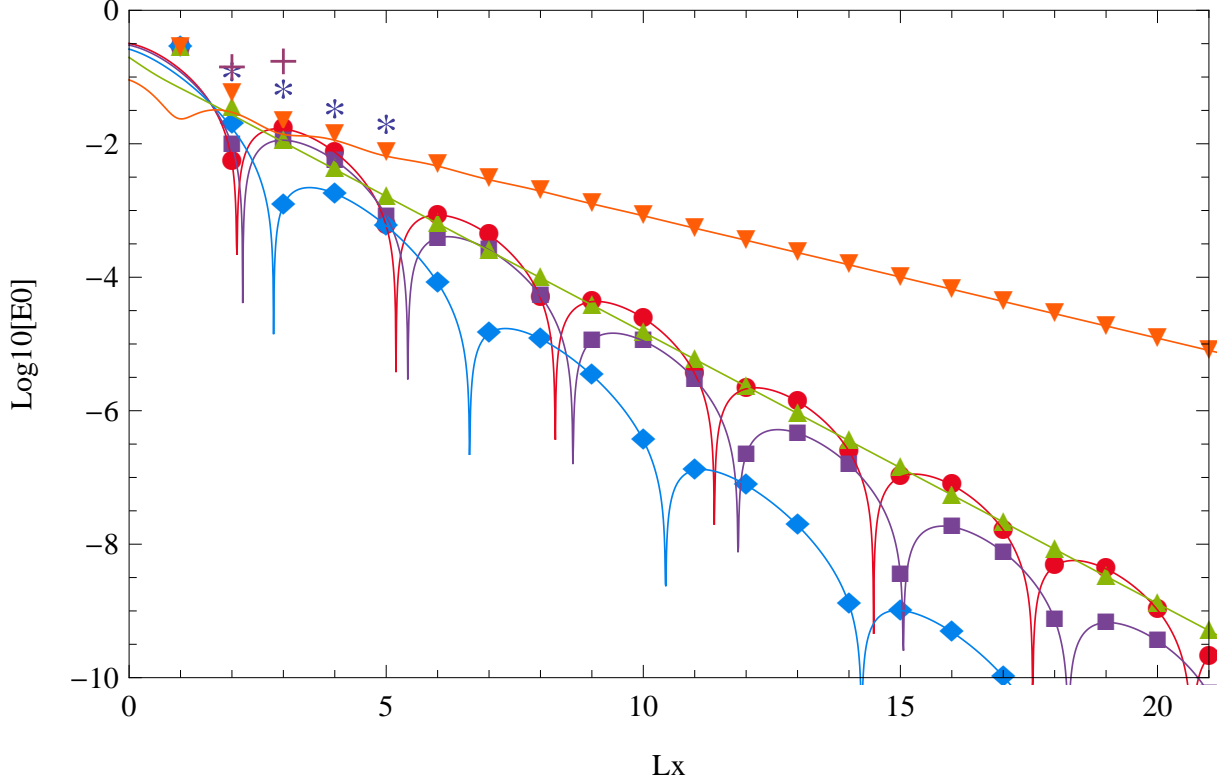


FIG. 4: Thickness (L_x) dependence of the (half) size energy gap E_0 in TI thin films. Comparison of $E_0(L_x)$ found by numerical diagonalization of the tight-binding Hamiltonian with open boundary conditions at $x = 1$ and $x = L_x$ [for a given set of model parameters this appears as a series of points with the same symbol and color], and the same dependence predicted by Eqs. (66) [shown as a continuous line in the same color]. For the series of filled red points the model parameters are chosen as given in Eqs. (68). In FIG. 2 this corresponds to a point $(m_0/m_{2x}, \tilde{t}_x/m_{2x}) = (-1.3, 1.51)$ as indicated by the same symbol and color. Other set of points correspond to $\epsilon_{2x}/m_{2x} = 0.3, 0.5, 0.7, 0.9$, *i.e.*, asymmetry in the spectrum of valence and conduction bands is enhanced from the original Bi_2Se_3 value. These set of points are all on the (dotted) line ($m_0/m_{2x} = -1.3$ in FIG. 2, while the value of effective hopping \tilde{t}_x varies as $\tilde{t}_x/m_{2x} = 1.57, 1.73, 2.10, 3.44$). The corresponding points are indicated by the same symbol and color in FIG. 2. Experimental values that have appeared in Refs.^{8,9} are also shown in the figure in plus and asterisk symbols for comparison.

the case of following model parameters deduced from material parameters of Bi_2Se_3 :²⁵

$$\begin{aligned} m_0 &= -0.28, \quad m_{2x} = 0.216, \\ \epsilon_0 &= -0.0083, \quad \epsilon_{2x} = 0.024, \\ t_x &= 0.32, \end{aligned} \tag{68}$$

in units of eV. In the original 3D bulk Hamiltonian, the remaining set of parameters:

$$\begin{aligned} m_{2y} &= m_{2z} = 2.6, \\ \epsilon_{2y} &= \epsilon_{2z} = 1.77, \\ t_y &= t_z = 0.8 \end{aligned} \tag{69}$$

are also relevant. The set of parameters specified by Eqs. (68) correspond in the phase diagram of FIG. 2 to a point $(m_0/m_{2x}, \tilde{t}_x/m_{2x}) = (-1.3, 1.51)$, denoted in the figure by a filled red circle, which falls on the “TI-oscillatory” phase, exhibiting a surface state with a damped oscillatory wave function. Note that the phase boundary between the TI-oscillatory and TI-overdamped phases is a circle represented by Eq. (54) in the $(m_0/m_{2x}, \tilde{t}_x/m_{2x})$ -plane, while the magnitude of the effective hopping \tilde{t}_x given in Eq. (45) is a function of ϵ_{2x} . Note that ϵ_{2x} encodes asymmetry of the spectrum in the valence and conduction bands. This signifies that one can drive the system from the original TI-oscillatory to the TI-overdamped phase by tuning the asymmetry parameter ϵ_{2x} .

In FIG. 4 we show the thickness (L_x) dependence of the (half) size gap E_0 calculated by numerical diagonalization of the tight-binding Hamiltonian with open boundary conditions at $x = 0$ and $x = L_x + 1$, superposed on the

same dependence predicted by Eqs. (66). The value of the parameter ϵ_{2x}/m_{2x} is varied from its original value $\epsilon_{2x}/m_{2x} = 0.11$ to $\epsilon_{2x}/m_{2x} = 0.3, 0.5, 0.7, 0.9$, which leads, respectively, to the value of $\tilde{t}_x/m_{2x} = 1.57, 1.73, 2.10, 3.44$. The corresponding point in the $(m_0/m_{2x}, \tilde{t}_x/m_{2x})$ -plane is specified in FIG. 2, respectively, by a filled square in purple ($\epsilon_{2x}/m_{2x} = 0.3$), a rhombus painted in light blue ($\epsilon_{2x}/m_{2x} = 0.5$), a upper green triangle ($\epsilon_{2x}/m_{2x} = 0.7$) and a lower orange triangle ($\epsilon_{2x}/m_{2x} = 0.9$). In FIG. 4 the L_x -dependence of E_0 at these values of the parameter ϵ_{2x}/m_{2x} is indicated by points represented by the same symbol and color. The corresponding theoretical curve specified by Eq. (66) is superposed on the same figure indicated by a continuous curve of the same color. Since the phase boundary between TI-oscillatory and TI-overdamped phases is located at $\tilde{t}_x/m_{2x} = 1.8735$ on the line $m_0/m_{2x} = -1.3$, L_x -dependence of E_0 also shows a crossover from a damped oscillation (for $\epsilon_{2x}/m_{2x} = 0.11, 0.3, 0.5$) to overdamping (for $\epsilon_{2x}/m_{2x} = 0.7, 0.9$). This feature, together with an excellent agreement between the numerical values of E_0 and Eq. (66), is highlighted in FIG. 4.

In FIG. 4 the size of energy gap determined experimentally for Bi_2Se_3 nanofilms (reported in Refs.^{8, 9}) is also shown for comparison with our theoretical results. It is curious that those of Ref.⁹ (indicated in asterisks) shows seemingly a monotonic decay as a function of the thickness of the film, while those of Ref.⁸ (indicated in pluses) seem to suggest an oscillatory behavior. We also note that these experimental values are generally larger than the theoretical predictions.

VII. CONCLUSIONS

Motivated by experimental realization of the topological insulator thin films, we have studied theoretically possible size effects on the protected surface Dirac state on such films. Indeed, finite thickness of the film induces coupling between the two Dirac cones; one at the top, the other at the bottom surface of the film (= a slab-shaped sample of a 3D TI). To quantify such finite-size effects we introduce a 1D effective model of a topological insulator, in which the spatial coordinate represents the direction of the depth, *i.e.*, the direction vertical to the surface of the film. Using this effective 1D model, we reveal a precise correspondence between the thickness dependence of the size gap and the spatial profile of the surface wave function in the semi-infinite geometry. In Sec. IV we solved the boundary problem in the semi-infinite geometry. This allows for, *e.g.*, determining exactly the energy at which the surface Dirac point appears. We then use this solution to study how the Dirac cone becomes gapped in the case of a slab with a finite thickness.

As shown in the phase diagram depicted in FIG. 2 the topologically nontrivial phase of our 1D model Hamiltonian, prescribed by Eqs. (9), (10) and (11), is divided into two subregions: the TI-oscillatory and the TI-overdamped phases. This effective model is deduced from a more realistic 3D effective Hamiltonian [specified by Eqs. (1), (2) and (3)] that successfully describes various topological features observed, *e.g.*, on cleaved surfaces of the Bi_2Se_3 crystal. In such original 3D bulk TI, asymmetry in the spectrum of valence and conduction bands is omnipresent. Here, we have demonstrated that by tuning this asymmetry one can drive [since tuning ϵ_{2x} leads to changing the effective hopping \tilde{t}_x given in Eq. (45)] a crossover from the TI-oscillatory to the TI-overdamped phase. We have also established analytic formulas for the the thickness (L_x) dependence of the size gap $2E_0$ [Eq. (66)] and a precise relation relation [Eq. (67)] between $E_0(L_x)$ and $\psi_{\text{semi}}(x)$, the surface wave function in the semi-infinite geometry [Eqs. (52), (53)]. Finally, Eqs. (45), (54), (66) and (67), together with FIG. 2 and FIG. 4 constitute the central results of the paper.

Acknowledgments

M.O. and K.I. thank useful discussion with Shuichi Murakami, Ai Yamakage and Takahiro Fukui. K.I. also acknowledges Toru Hirahara, Koji Segawa, Yasuhiro Tada and Norio Kawakami for correspondences. Y.T. is supported by Grants-in-Aid for Scientific Research (C) [No. 24540375] from Japan Society for the Promotion of Science.

-
- ¹ L. Fu, C. L. Kane, and E. J. Mele, Phys. Rev. Lett. **98**, 106803 (2007), URL <http://link.aps.org/doi/10.1103/PhysRevLett.98.106803>.
² L. Fu and C. L. Kane, Phys. Rev. B **76**, 045302 (2007), URL <http://link.aps.org/doi/10.1103/PhysRevB.76.045302>.
³ J. E. Moore and L. Balents, Phys. Rev. B **75**, 121306 (2007), URL <http://link.aps.org/doi/10.1103/PhysRevB.75.121306>.
⁴ R. Roy, Phys. Rev. B **79**, 195322 (2009), URL <http://link.aps.org/doi/10.1103/PhysRevB.79.195322>.
⁵ J. E. Moore, Nature (London) **464**, 194 (2010).
⁶ M. Z. Hasan and C. L. Kane, Rev. Mod. Phys. **82**, 3045 (2010).
⁷ X.-L. Qi and S.-C. Zhang, Rev. Mod. Phys. **83**, 1057 (2011).

- ⁸ Y. Sakamoto, T. Hirahara, H. Miyazaki, S.-i. Kimura, and S. Hasegawa, Phys. Rev. B **81**, 165432 (2010), URL <http://link.aps.org/doi/10.1103/PhysRevB.81.165432>.
- ⁹ Y. Zhang, K. He, C.-Z. Chang, C.-L. Song, L.-L. Wang, X. Chen, J.-F. Jia, Z. Fang, X. Dai, W.-Y. Shan, et al., Nature Physics **6**, 584 (2010).
- ¹⁰ A. A. Taskin, S. Sasaki, K. Segawa, and Y. Ando, Phys. Rev. Lett. **109**, 066803 (2012), URL <http://link.aps.org/doi/10.1103/PhysRevLett.109.066803>.
- ¹¹ A. A. Taskin, S. Sasaki, K. Segawa, and Y. Ando, Advanced Materials **24**, 5581 (2012), ISSN 1521-4095, URL <http://dx.doi.org/10.1002/adma.201201827>.
- ¹² A. A. Taskin, S. Sasaki, K. Segawa, and Y. Ando, ArXiv e-prints (2013), 1305.2470.
- ¹³ B. Zhou, H.-Z. Lu, R.-L. Chu, S.-Q. Shen, and Q. Niu, Phys. Rev. Lett. **101**, 246807 (2008), URL <http://link.aps.org/doi/10.1103/PhysRevLett.101.246807>.
- ¹⁴ H.-Z. Lu, W.-Y. Shan, W. Yao, Q. Niu, and S.-Q. Shen, Phys. Rev. B **81**, 115407 (2010), URL <http://link.aps.org/doi/10.1103/PhysRevB.81.115407>.
- ¹⁵ J. Linder, T. Yokoyama, and A. Sudbø, Phys. Rev. B **80**, 205401 (2009), URL <http://link.aps.org/doi/10.1103/PhysRevB.80.205401>.
- ¹⁶ W.-Y. Shan, H.-Z. Lu, and S.-Q. Shen, New Journal of Physics **12**, 043048 (2010), URL <http://stacks.iop.org/1367-2630/12/i=4/a=043048>.
- ¹⁷ C.-X. Liu, H. Zhang, B. Yan, X.-L. Qi, T. Frauenheim, X. Dai, Z. Fang, and S.-C. Zhang, Phys. Rev. B **81**, 041307 (2010), URL <http://link.aps.org/doi/10.1103/PhysRevB.81.041307>.
- ¹⁸ K.-I. Imura, M. Okamoto, Y. Yoshimura, Y. Takane, and T. Ohtsuki, Phys. Rev. B **86**, 245436 (2012), URL <http://link.aps.org/doi/10.1103/PhysRevB.86.245436>.
- ¹⁹ C.-X. Liu, X.-L. Qi, H. Zhang, X. Dai, Z. Fang, and S.-C. Zhang, Phys. Rev. B **82**, 045122 (2010).
- ²⁰ H. Zhang, C.-X. Liu, X.-L. Qi, X. Dai, Z. Fang, and S.-C. Zhang, Nature Physics **5**, 438 (2010).
- ²¹ A. P. Schnyder, S. Ryu, A. Furusaki, and A. W. W. Ludwig, Phys. Rev. B **78**, 195125 (2008), URL <http://link.aps.org/doi/10.1103/PhysRevB.78.195125>.
- ²² S. Ryu, A. P. Schnyder, A. Furusaki, and A. W. W. Ludwig, New Journal of Physics **12**, 065010 (2010), URL <http://stacks.iop.org/1367-2630/12/i=6/a=065010>.
- ²³ A. Kitaev, AIP Conference Proceedings **1134**, 22 (2009), URL <http://link.aip.org/link/?APC/1134/22/1>.
- ²⁴ A. P. Schnyder, S. Ryu, A. Furusaki, and A. W. W. Ludwig, AIP Conference Proceedings **1134**, 10 (2009), URL <http://link.aip.org/link/?APC/1134/10/1>.
- ²⁵ K. Ebihara, K. Yada, A. Yamakage, and Y. Tanaka, Physica E: Low-dimensional Systems and Nanostructures **44**, 885 (2012), ISSN 1386-9477, URL <http://www.sciencedirect.com/science/article/pii/S1386947711004413>.
- ²⁶ It is sometimes convenient to measure everything in units of m_{2x} .